Sensor Radar Networks for Indoor Tracking

Stefania Bartoletti, *Student Member, IEEE*, Andrea Conti, *Senior Member, IEEE*, Andrea Giorgetti, *Senior Member, IEEE*, and Moe Z. Win, *Fellow, IEEE*

***Abstract*—Sensor radars (SRs) are important for a variety of applications requiring passive tracking of moving targets. The accuracy of passive tracking is severely degraded by wireless propagation impairments such as multipath, clutter, and non line-of-sight conditions, especially in indoor environments. These impairments can be alleviated by exploiting the multiple sensing and smart processing of radar signals. In this letter, we aim to illustrate the dependence of sensor topologies, waveform processing methods, and tracking algorithm parameters on SR performance. A case study involving both monostatic and multistatic ultra-wideband SRs for indoor environments is presented by jointly considering the wireless medium, ranging technique, and tracking algorithm.**

***Index Terms*—Sensor radar, indoor tracking, UWB, TOA estimation.**

I. Introduction

TRACKING of moving targets (objects, persons, and vehicles) enables several applications in military, security, and safety sectors. While active tracking relies on targets that emit signals, passive tracking via sensor radars (SRs) relies on a network of sensors that emit radar signals and receive them after backscattering from the target [1]–[3]. The inference of target position, which is based on the joint processing of received waveforms and prior knowledge, is particularly challenging in indoor environments, where multipath, clutter, and non-line-of-sight (NLOS) conditions affect the received waveforms.

The literature considers SRs to be a low-power and low-complexity solution for accurate detection and tracking of moving targets. Recently, ultra-wideband (UWB) SRs have gained interest owing to their ability to resolve multipaths and penetrate obstacles [4]–[6]. It has been shown that UWB SRs can provide submeter tracking accuracy even in harsh indoor environments [7]–[9].

The fundamental question related to passive tracking via SRs under complexity constraints is the following: how to design the network (e.g., sensor positions and radar configurations) and to allocate the processing (e.g., ranging and tracking) resources for different tasks? The answers to this question will provide insights into the efficient design of high accuracy SRs. The goal of this letter is to illustrate the SR performance improvement that can be obtained by properly designing the radar network and allocating the processing resources. Previous works on SRs separately investigated the following aspects: sensor positions [10], wireless propagation [11], ranging techniques [12], and tracking algorithms [13]. Our view is that the joint design of radar network, waveform processing, and tracking algorithm can significantly improve the SR performance.

This letter explores SRs by considering network configuration, propagation impairments, as well as ranging and tracking techniques. We provide a case study in indoor environments (with obstructions, clutter, and multipath) and quantify the performance (tracking error and outage) of monostatic and multistatic UWB SRs for different settings. The case study provides insights into the joint design of networking and processing for SRs operating in challenging environments.

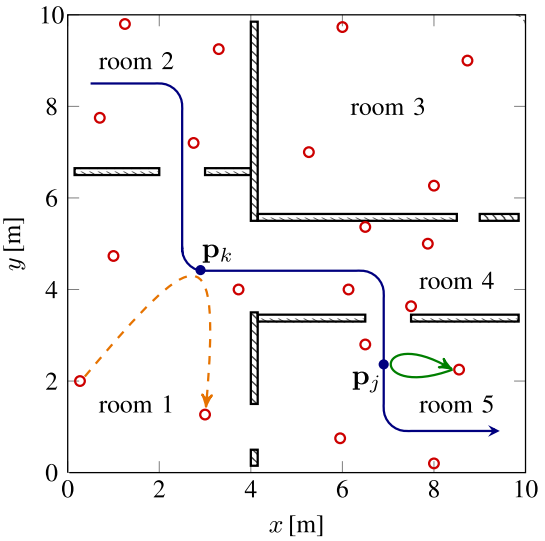

Fig. 1. An example of SR deployment (red circles) and of a target trajectory (solid blue line). The blue dots indicate target positions at time indexes k and j. Continuous green and dashed brown arrows exemplify a transmitter-target-receiver radar signal for monostatic and multistatic configuration, respectively.

II. Networking and Propagation

Consider an SR (see e.g., Fig. 1) composed of N_s sensors, of which N_t serve as transmitters and N_r serve as receivers.[1] The radar configuration is monostatic or multistatic depending on whether transmitters and receivers are co-located or not.

[1] The discrimination among different transmitted UWB signals can be performed by timehopping (TH) and/or direct-sequence (DS) codes [4].

Manuscript received October 31, 2013. The associate editor coordinating the review of this letter and approving it for publication was I. Guvenc.

S. Bartoletti and A. Conti are with ENDIF, University of Ferrara, (e-mail: stefania.bartoletti@unife.it, a.conti@ieee.org).

A. Giorgetti is with DEI, University of Bologna, (e-mail: a.giorgetti@ieee.org).

M. Z. Win is with LIDS, Massachusetts Institute of Technology, (e-mail: moewin@mit.edu).

This research was supported, in part, by the Italian MIUR within the project GRETA under Grant 2010WHY5PR, the University of Ferrara under Grant 5x1000 2010 and UNICREDIT 2013, the Air Force Office of Scientific Research under Grant FA9550-12-0287, and the MIT Institute for Soldier Nanotechnologies.

Digital Object Identifier 10.1109/WCL.2013.120513.130760

The radar configuration determines the index set $\mathcal{P}$ of transmitter-receiver pairs, where each $(i,j) \in \mathcal{P}$ denotes the ith transmitter emitting radar signals and the jth receiver collecting them after backscattering from the target. For a target position $\mathbf{p}_k \in \mathbb{R}^d$ at time k, the signal path-length is given by $d_{ij}(\mathbf{p}_k)$, which is the distance from the ith transmitter to the target to the jth receiver. The range estimate results in $\hat{d}_{ij}(\mathbf{p}_k) = \hat{\tau}_{ij}(\mathbf{p}_k)\, c$, where c is the speed of light and $\hat{\tau}_{ij}(\mathbf{p}_k)$ is the estimated time-of-arrival (TOA) of a backscattered signal, at the jth receiver, emitted by the ith transmitter [14]. We denote τ_{min} as the minimum resolvable delay for the multistatic case and as the blind temporal range for the monostatic case.[2]

The accuracy of TOA estimation depends on radar signal propagation, which is affected by multipath, clutter, and obstructions. Specifically, when the target is at $\mathbf{p}_k$, the received signal-to-noise ratio (SNR) is given by

$$\gamma_{ij}(\mathbf{p}_k) = P_{\text{R},ij}(\mathbf{p}_k)\, T_{\text{pr}}/N_0 \tag{1}$$

where $P_{\text{R},ij}(\mathbf{p}_k)$ is the received power per pulse, T_{pr} is the pulse repetition period (PRP), and N_0 is the one-sided power spectral density (PSD) of the noise. The TOA can be estimated if the received SNR is above a value $\gamma^\star$, which corresponds to the minimum required received power per pulse $P_{\text{R}}^\star$.[3]

For UWB signals propagating in indoor environments, we determine the received power as in [9] and model the obstruction-loss accounting for the number and the type (i.e., electromagnetic characteristics) of obstructions in the transmitter-to-target-to-receiver path, as in [15]. Note that the presence of objects and walls obstructing the signal path also causes an excess delay in the TOA estimates. We quantify these effects based on experimentations performed in a typical building [16]. In particular, the walls cause a positive bias $\mu_{ij}(\mathbf{p}_k) \simeq \Delta/c$ on the TOA estimate, where Δ is the aggregate thickness of the walls.

III. Signal Processing

We now describe signal processing to infer target positions. First, received radar waveforms are processed to determine transmitter-target-receiver distances based on TOA estimation. Then, such radar ranging information is used to infer target positions based on the tracking algorithm.

A. TOA Estimation

We consider TOA estimation based on an energy detector (ED), which is amenable to efficient low-complexity implementation for UWB ranging [12]. Before energy detection, received waveforms are processed by a band-pass filter and clutter mitigation techniques. The signal at the input of the ED is

$$v_{ij}(t) = \sum_{p=0}^{N_{\text{p}}-1} \sum_{l=1}^{L_{\text{p}}} \alpha_{ij}^{(l)}\, s(t - p\,T_{\text{pr}} - \tau_{ij}^{(l)}) + n_{ij}(t) \tag{2}$$

where N_{p} is the number of transmitted pulses, L_{p} is the number of multipath components (with amplitude $\alpha_{ij}^{(l)}$ and delay $\tau_{ij}^{(l)}$ for the lth component), $s(t)$ is the filtered pulse shape, and $n_{ij}(t)$ is the filtered noise. The TOA to be estimated is that of the first path (i.e., $\tau_{ij}(\mathbf{p}_k) = \tau_{ij}^{(1)}$).[4] Target detection and TOA estimation are performed by collecting $N_{\text{bin}} = \lfloor T_{\text{pr}}/T_{\text{d}} \rfloor$ energy bins, where T_{d} is the dwell time.[5] Then, the decision vector $\overline{\boldsymbol{\epsilon}}_{ij} = \left(\overline{\epsilon}_{ij}^{(0)}, \overline{\epsilon}_{ij}^{(1)}, \ldots, \overline{\epsilon}_{ij}^{(N_{\text{bin}}-1)}\right)$ is obtained by averaging each energy bin over the N_{p} transmitted pulses. Each $\overline{\epsilon}_{ij}^{(q)}$ is then compared with a threshold ξ_{ij}, and the first crossing event provides the TOA estimate [12], [17]. The threshold value strongly influences TOA estimation and needs to be carefully designed according to the operating conditions.

B. Tracking Algorithm

The tracking algorithm infers the target position $\mathbf{p}_k$ at each time index k (i.e., the current state vector) from a set of TOA estimates (i.e., observations), a mobility model (i.e., relation between the current and the prior state vectors), and a perception model (i.e., relation between the observations and the current state vector [1]. Following a Bayesian approach, the position estimate $\hat{\mathbf{p}}_k$ is determined as the value that maximizes the positional belief $b(\mathbf{p}_k) = p(\mathbf{p}_k|\hat{\boldsymbol{\tau}}_{\mathcal{P}_{\text{sel}}}(\mathbf{p}_{1:k}))$, which is the posterior distribution of the state vector, conditioned on a subset of observations $\hat{\boldsymbol{\tau}}_{\mathcal{P}_{\text{sel}}}(\mathbf{p}_{1:k})$ with $\mathcal{P}_{\text{sel}} \subseteq \mathcal{P}$, i.e. $\hat{\mathbf{p}}_k = \text{argmax}_{\mathbf{p}_k}\, b(\mathbf{p}_k)$.[6] In particular, the positional belief is

$$b(\mathbf{p}_k) \propto p\left(\hat{\boldsymbol{\tau}}_{\mathcal{P}_{\text{sel}}}(\mathbf{p}_{1:k})|\mathbf{p}_k\right) \times p\left(\mathbf{p}_k|\hat{\boldsymbol{\tau}}_{\mathcal{P}_{\text{sel}}}(\mathbf{p}_{1:k-1})\right) \tag{3}$$

where the first term $p\left(\hat{\boldsymbol{\tau}}_{\mathcal{P}_{\text{sel}}}(\mathbf{p}_{1:k})|\mathbf{p}_k\right)$ is the perception model. The second term $p\left(\mathbf{p}_k|\hat{\boldsymbol{\tau}}_{\mathcal{P}_{\text{sel}}}(\mathbf{p}_{1:k-1})\right)$ is given by $\int p(\mathbf{p}_k|\mathbf{p}_{k-1})\, p\left(\mathbf{p}_{k-1}|\hat{\boldsymbol{\tau}}_{\mathcal{P}_{\text{sel}}}(\mathbf{p}_{1:k-1})\right) d\mathbf{p}_{k-1}$ where $p(\mathbf{p}_k|\mathbf{p}_{k-1})$ is the mobility model. The subset of selected observations $\mathcal{P}_{\text{sel}}$ is chosen based on a selection criterion [18]. Specifically, in the case study we select the $|\mathcal{P}_{\text{sel}}| = 3$ observations that provided the maximum received power, i.e., $\min\{P_{\text{R},\mathcal{P}_{\text{sel}}}\} \geq \max\{P_{\text{R},\mathcal{P}\setminus\mathcal{P}_{\text{sel}}}\}$.

Among the common implementations of Bayesian algorithms, we consider the particle filter (PF) algorithm, which can outperform extended Kalman filter (EKF) in non-Gaussian noisy observations [13].[7] In particular, the positional belief at time k is represented by a set of N_{par} random samples (particles) at $\{\mathbf{p}_k^{(n)}\}$, with $n = 1, 2, ..., N_{\text{par}}$. The mobility and perception models are used to predict, update, and resample the positional belief at each k. In particular, a Gaussian mobility model is given by $\mathbf{p}_k^{(n)}|\mathbf{p}_{k-1}^{(n)} \sim \mathcal{N}(\boldsymbol{\mu}_k^{(n)}, \sigma_{\text{m},k}^2\,\mathbf{I})$, where $\mathbf{I}$ is the identity matrix and $\sigma_{\text{m},k}^2$ depends on the target mobility.[8] The mean $\hat{\boldsymbol{\mu}}_k^{(n)}$ is determined based on previous position estimates as $\hat{\boldsymbol{\mu}}_k^{(n)} = \mathbf{p}_{k-1}^{(n)} + \hat{\mathbf{v}}_k\, T_{\text{L}}$, where $\hat{\mathbf{v}}_k$ is the average speed calculated over N_{w} previous positions, and T_{L} is the time between two position estimations. A perception

[2]The τ_{min} is determined by the relative delay between the backscattered signal and the direct signal for multistatic configuration, and by the switching time between transmitting and receiving modes for monostatic configuration.

[3]We consider the target in $\mathbf{p}_k$ as detected if $\exists (i,j) \in \mathcal{P}$ s.t. $P_{\text{R},ij}(\mathbf{p}_k) > P_{\text{R}}^\star$ (i.e., at least one TOA estimation can be performed).

[4]We consider that $\tau_{ij}^{(1)}$ is in the range $[\tau_{\text{min}}, T_{\text{a}}]$, where T_{a} is the greatest possible TOA value in the environment and T_{pr} is chosen such that $T_{\text{pr}} > T_{\text{a}}$.

[5]The notation $\lfloor x \rfloor$ denotes the largest integer not greater than x.

[6]$\hat{\boldsymbol{\tau}}_{\mathcal{P}_{\text{sel}}}(\mathbf{p}_{1:k}) \triangleq \{\hat{\tau}_{ij}(\mathbf{p}_h)$ s.t. $(i,j) \in \mathcal{P}_{\text{sel}}, h = 1, 2, ..., k\}$.

[7] Note that, in general, the observations follow a non-Gaussian distribution due to multipath and clutter residual.

[8]$\mathcal{N}(\boldsymbol{\mu}, \boldsymbol{\sigma}^2)$ denotes the d-dimensional Gaussian distribution with mean $\boldsymbol{\mu}$ and variance $\boldsymbol{\sigma}^2$.

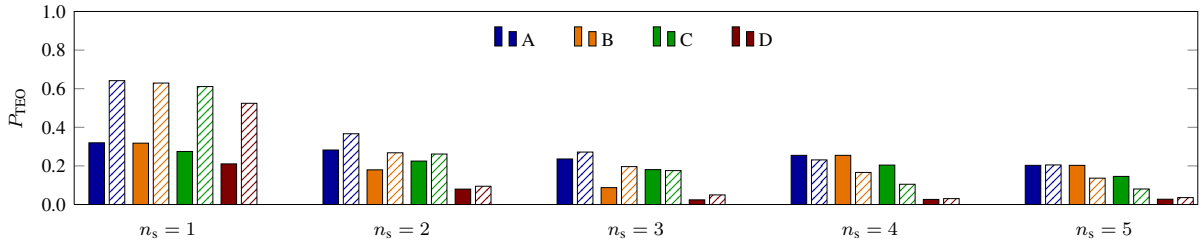

Fig. 2. TEO for $e_{\text{th}} = 1\text{m}$, $T_{\text{d}} = 2\,\text{ns}$, and varying number of sensors per room n_{s}. The processing configurations A, B, C, D are considered for monostatic (uniform pattern) and multistatic (dashed pattern) networking.

model for particles with independent observations, is given by

$$p(\hat{\boldsymbol{\tau}}_{\mathcal{P}_{\text{sel}}}(\mathbf{p}_k)|\mathbf{p}_k^{(n)}) = \prod_{(i,j)\in\mathcal{P}_{\text{sel}}} \frac{1}{\sqrt{2\pi}\sigma_{\text{p},k}} e^{-\frac{\left[\hat{\tau}_{ij}(\mathbf{p}_k)\,c - d_{ij}(\mathbf{p}_k^{(n)})\right]^2}{2\sigma_{\text{p},k}^2}}$$

where $\sigma_{\text{p},k}^2$ depends on ranging and propagation.

IV. Case Study

We first describe the operating environment and then evaluate the performance of monostatic and multistatic SRs.

A. Operating Environment

We consider SRs with UWB impulse radios deployed in the operating environment shown in Fig. 1 with wall thickness of 15 cm. In the monostatic configuration, each sensor transmits and receives ($N_{\text{t}} = N_{\text{s}}$). In the multistatic configuration, one sensor per room transmits ($N_{\text{t}} = 5$); specifically, the sensor closest to $\hat{\mathbf{p}}_{k-1}$ transmits at time $k > 1$ (random at $k = 1$). We consider the target speed $|\mathbf{v}| = 1$ m/s along 10 trajectories with $T_{\text{L}} = 0.5$ s. We evaluate the performance for $N_{\text{s}} = 5, 10, ..., 25$ sensors (i.e., $n_{\text{s}} = 1, 2, ..., 5$ sensors per room, respectively).[9]

Transmitters emit a sequence of root raised cosine (RRC) pulses with $T_{\text{pr}} = 200\,\text{ns}$ and transmitted PSD compliant with the European lower band. The transmitted PSDs for the monostatic and multistatic configurations are set to have the same total transmitted power. We consider $P_{\text{R}}^{\star} = -110\,\text{dBm}$ and $N_0 = -200\,\text{dBW/Hz}$. The channel impulse response is modeled with $L_{\text{p}} = 20$ paths spaced by $\delta_{\text{p}} = 4\,\text{ns}$, exponential power delay profile with decay constant $\epsilon = 20$ ns, and Nakagami-2 distributed path amplitudes. The target radar cross section (RCS) is Swerling type III distributed with mean $1\,\text{m}^2$ (typical for the human body) [14]. The ED-based TOA estimates $\hat{\boldsymbol{\tau}}_{\mathcal{P}}(\mathbf{p}_k)$ are obtained with $T_{\text{d}} = 1, 2, 4\,\text{ns}$ and $N_{\text{p}} = 32, 128$. A best-case analysis for ED-based ranging is provided by considering the threshold ξ_{ij} that minimizes the root-mean-square error (RMSE) of TOA estimates for each received SNR value.

Static clutter is generated using 100 scatterers for each transmitter-receiver pair, with uniformly distributed TOAs and a Swerling type V distributed RCS with mean $1\,\text{m}^2$. The empty-room technique is employed for clutter mitigation [19]. Specifically, a reference waveform is subtracted from the received waveform for each transmitter-receiver pair. This reference waveform is obtained by averaging 100 received waveforms in the absence of target. The tracking algorithm is based on PF with $N_{\text{par}} = 100$ and 1000, $\sigma_{\text{p},k}^2 = 1$ for all k, and $N_{\text{w}} = 2$. The value of $\sigma_{\text{m},k}^2$ is chosen such that the nth estimated particle at time k is within a circle centered at $\hat{\boldsymbol{\mu}}_k^{(n)}$ of radius $|\hat{\mathbf{v}}_k|\,T_{\text{L}}$ with probability 0.9. When the selection of observations is performed, the set $\hat{\boldsymbol{\tau}}_{\mathcal{P}_{\text{sel}}}$ includes three observations $|\mathcal{P}_{\text{sel}}| = 3$ corresponding to the signals received with the highest power; otherwise it includes all the available TOA estimates $|\mathcal{P}_{\text{sel}}| = |\mathcal{P}|$.

B. Performance Evaluation

We now quantify the tracking performance in the indoor environment shown in Fig. 1 by simulating several configurations of the network and varying the setting of signal processing.[10] Specifically, we determine the effects of (i) network topology by employing monostatic and multistatic SR with $n_{\text{s}} = 2, 3, 4$, and 5 sensors; (ii) TOA estimation by collecting $N_{\text{pulse}} = 32$ and 128 pulses for energy detection with $T_{\text{d}} = 1, 2$, and 4 ns; (iii) tracking algorithm by sampling with $N_{\text{par}} = 100$ and 1000 particles; and (iv) selection of observations by considering all the available observations or a subset of them. Four processing settings are considered: (A) $N_{\text{pulse}} = 32$, $N_{\text{par}} = 100$, and $|\mathcal{P}_{\text{sel}}| = |\mathcal{P}|$; (B) $N_{\text{pulse}} = 32$, $N_{\text{par}} = 100$, and $|\mathcal{P}_{\text{sel}}| = 3$; (C) $N_{\text{pulse}} = 32$, $N_{\text{par}} = 1000$, and $|\mathcal{P}_{\text{sel}}| = |\mathcal{P}|$; and (D) $N_{\text{pulse}} = 128$, $N_{\text{par}} = 100$, and $|\mathcal{P}_{\text{sel}}| = |\mathcal{P}|$. Note that cases B, C, and D differ from A for the values of $|\mathcal{P}_{\text{sel}}|$, N_{par}, and N_{pulse}, respectively. Tracking performance is evaluated in terms of tracking error, i.e., the Euclidean distance between the estimated and the true position, tracking RMSE, and tracking error outage (TEO), i.e., the probability that tracking error is above a given value e_{th}.[11]

Figure 2 shows the TEO for monostatic and multistatic configurations with $e_{\text{th}} = 1\,\text{m}$, $T_{\text{d}} = 2\,\text{ns}$, and different n_{s} values. It can be seen that, in each setting, the TEO tends to decrease as n_{s} increases, with negligible improvement for $n_{\text{s}} > 3$. Moreover, the multistatic configuration is more sensitive to the number of sensors per room. For example in setting A, varying n_{s} from 1 to 5 reduces the TEO from 0.31 to 0.20 with the monostatic SR, whereas it reduces the TEO from 0.64 to 0.20 with the multistatic SR. In the setting D,

[9]The n_{s} sensors are deployed on a circle inscribed in each room, equally spaced from each other, and with initial angle $\pi/6$.

[10]The main impairments affecting SR performance are taken into account, even though additional phenomena might occur in real scenarios.

[11]The TEO is evaluated over 10 trajectories each with 100 realizations of random processes.

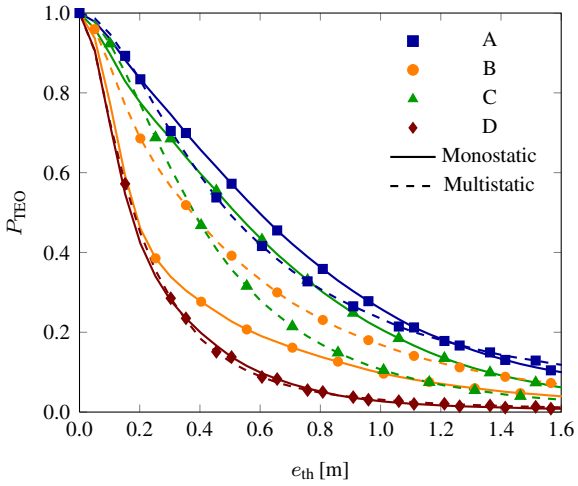

Fig. 3. TEO as a function of e_{th} for the cases A, B, E, and F, with $N_{\text{s}} = 20$ (i.e., $n_{\text{s}} = 4$) sensors in monostatic or multistatic configuration.

the TEO reduces from 0.21 to 0.02 for the monostatic SR and from 0.52 to 0.03 for the multistatic SR. Figure 2 also shows that multistatic SR experiences a higher TEO than monostatic SR at low values of n_{s} because the number of line-of-sight (LOS) conditions is smaller for the former than the latter.

Figure 3 shows the TEO as a function of e_{th} for $T_{\text{d}} = 2\,\text{ns}$ with $N_{\text{s}} = 20$. It can be seen that TEO benefits more from a larger number of pulses collected for ranging than from a larger number of particles used for tracking. For $e_{\text{th}} = 0.5\,\text{m}$, varying the processing from setting A to C or D changes the TEO from 0.57 to 0.51 or 0.14 with the monostatic SR and from 0.49 to 0.36 or 0.12 with the multistatic, respectively. Moreover, especially for monostatic SR, results obtained with $|\mathcal{P}_{\text{sel}}| = 3$ and $N_{\text{pulse}} = 32$ are comparable with those obtained with $|\mathcal{P}_{\text{sel}}| = 3$ and $N_{\text{pulse}} = 128$. Therefore, given N_{s} and e_{th}, the selection allows the collection of a lower number of pulses.

To investigate the effect of dwell time on the RMSE, Table I lists the tracking RMSE when $N_{\text{pulse}} = 128$, $N_{\text{par}} = 1000$, $|\mathcal{P}_{\text{sel}}| = 3$, $T_{\text{d}} = 1, 2$, and $4\,\text{ns}$, and with different numbers of sensors per room. Note that, for a given value of N_{pulse}, reducing T_{d} is less effective than increasing the number of n_{s}.

V. Conclusion

We characterized the effects of radar networking and signal processing on the tracking accuracy of SRs operating in indoor environments. The results show that submeter accuracy can be achieved with a proper allocation of resources. In particular, deploying more than three sensors per room increases the network cost without contributing significantly to localization accuracy. We also observed that the monostatic SRs perform better than the multistatic ones when resources are severely limited, while the multistatic SRs perform better than the monostatic ones not when ample resources are available. Moreover, a smart selection of available observations can improve performance, especially when a large number of sensors is deployed. The results in this letter provide guidelines for the joint design of the radar network, waveform processing, and tracking algorithm for inferring the position of moving targets in indoor scenarios.

TABLE I

Tracking RMSE for $N_{\text{pulse}} = 128$, $N_{\text{par}} = 1000$, and $|\mathcal{P}_{\text{sel}}| = 3$ varying n_{s}, T_{d} [ns], and network configuration.

	Monostatic			Multistatic		
n_{s} \ T_{d}	4	2	1	4	2	1
1	1.12	1.31	0.97	14.41	14.41	14.41
2	0.63	0.55	0.57	0.88	0.73	0.78
3	0.30	0.21	0.39	0.48	0.40	0.35
4	0.28	0.24	0.20	0.35	0.30	0.26
5	0.30	0.22	0.20	0.40	0.29	0.32

References

[1] M. Z. Win, A. Conti, S. Mazuelas, Y. Shen, W. M. Gifford, D. Dardari, and M. Chiani, "Network localization and navigation via cooperation," *IEEE Commun. Mag.*, vol. 49, no. 5, pp. 56–62, May 2011.

[2] F. Viani, P. Rocca, G. Oliveri, D. Trinchero, and A. Massa, "Localization, tracking, and imaging of targets in wireless sensor networks: an invited review," *Radio Science*, vol. 46, no. 5, pp. 1–12, Oct. 2011.

[3] J. Shen, A. Molisch, and J. Salmi, "Accurate passive location estimation using TOA measurements," *IEEE Trans. Wireless Commun.*, vol. 11, no. 6, pp. 2182–2192, Jun. 2012.

[4] M. Z. Win and R. A. Scholtz, "Impulse radio: how it works," *IEEE Commun. Lett.*, vol. 2, no. 2, pp. 36–38, Feb. 1998.

[5] Y. Shen and M. Z. Win, "Fundamental limits of wideband localization–part I: a general framework," *IEEE Trans. Inf. Theory*, vol. 56, no. 10, pp. 4956–4980, Oct. 2010.

[6] L. Stoica, A. Rabbachin, and I. Oppermann, "A low-complexity noncoherent IR-UWB transceiver architecture with TOA estimation," *IEEE Trans. Microw. Theory Tech.*, vol. 54, no. 4, pp. 1637–1646, Jun. 2006.

[7] E. Paolini, A. Giorgetti, M. Chiani, R. Minutolo, and M. Montanari, "Localization capability of cooperative anti-intruder radar systems," *EURASIP J. Advances in Signal Process.*, vol. 2008, pp. 1–14, Apr. 2008.

[8] M. Arik and O. B. Akan, "Collaborative mobile target imaging in UWB wireless radar sensor networks," *IEEE J. Sel. Areas Commun.*, vol. 28, no. 6, pp. 950–961, Aug. 2010.

[9] S. Bartoletti, A. Giorgetti, and A. Conti, "UWB sensor radar networks for indoor passive navigation," in *Proc. 2012 Tyrrhenian Int. Workshop on Adv. in Radar and Remote Sens.*, pp. 1–6.

[10] I. Bradaric, G. T. Capraro, and M. C. Wicks, "Sensor placement for improved target resolution in distributed radar systems," in *Proc. 2008 IEEE Int. Radar Conference*, pp. 1–6.

[11] R. D'Errico, "An indoor backscattering channel characterization for UWB passive RFID applications," in *Proc. 2012 Europ. Conf. on Antennas and Propag.*, pp. 1169–1173.

[12] D. Dardari, A. Conti, U. J. Ferner, A. Giorgetti, and M. Z. Win, "Ranging with ultrawide bandwidth signals in multipath environments," *Proc. IEEE*, vol. 97, no. 2, pp. 404–426, Feb. 2009.

[13] F. Gustafsson, F. Gunnarsson, N. Bergman, U. Forsell, J. Jansson, R. Karlsson, and P. J. Nordlund, "Particle filters for positioning, navigation and tracking," *IEEE Trans. Signal Process.*, vol. 50, no. 2, pp. 425–437, Feb. 2002.

[14] M. I. Skolnik, *Radar Handbook*, 3rd ed. McGraw-Hill, 1970.

[15] A. Safaai-Jazi, S. Riad, A. Muqaibel, and A. Bayram, "Ultra-wideband propagation measurements and channel modeling; through-the-wall propagation and material characterization," *DARPA NETEX program*, 2002.

[16] A. Conti, M. Guerra, D. Dardari, N. Decarli, and M. Z. Win, "Network experimentation for cooperative localization," *IEEE J. Sel. Areas Commun.*, vol. 30, no. 2, pp. 467–475, Feb. 2012.

[17] A. Giorgetti and M. Chiani, "Time-of-arrival estimation based on information theoretic criteria," *IEEE Trans. Signal Process.*, vol. 61, no. 8, pp. 1869–1879, Apr. 2013.

[18] S. Bartoletti, A. Giorgetti, and A. Conti, "Sensor radars with subset diversity," in *Proc. 2013 IEEE Workshop on Advances in Network Localization and Navigation (ICC)*, pp. 1–5.

[19] S. Nag and M. Barnes, "A moving target detection filter for an ultra-wideband radar," in *Proc. 2003 IEEE Int. Radar Conf.*, pp. 147–153.